Electronic and magnetic structures in metallic thin films

K. Okazaki and Y. Teraoka
Department of Materials Science, College of Integrated Arts and Sciences, Osaka Prefecture University, Sakai 599-8531, Japan
(Received 11 January 1999)

Electronic and magnetic structures in metallic thin films are theoretically studied using the planar uniform jellium model on a basis of the spin density functional theory. The electron density, the spin density, and the effective potential are self-consistently calculated as functions of the film thickness D within a framework of the local spin density approximation. Several states, such as nonmagnetic (N), fully polarized ferromagnetic (FPF), partially polarized ferromagnetic (PPF), and antiferromagnetic (AF) states, are found as solutions of the Kohn-Sham equation. FPF and AF state have spin polarization over all the films, on the other hand, the spin polarization in PPF state is localized near the surfaces. It is found that an AF film with D consists of two FPF films with $D/2$. By comparing the total energies, the ground state is determined as a function of D: FPF at $D \leqslant 9.0$ (in the atomic unit), N at $9.0 < D \leqslant 11.9$, PPF at $11.9 < D \leqslant 12.8$, FPF at $12.8 < D \leqslant 16.4$, PPF at $16.4 < D \leqslant 17.1$, N at $17.1 < D \leqslant 22.1$, PPF at $22.1 < D \leqslant 25.6$, and N at $25.6 < D$ for $r_s = 6$, where r_s is the Wigner sphere radius. The ground state of a very thin film is FPF, whatever value the average electron density over the film takes. Alkali metal thin films, especially, Cs and Rb thin films are expected to be ferromagnetic.

I. INTRODUCTION

Low-dimensional magnetism, such as on surfaces, on interfaces, in thin films, and in very fine particles, is a matter of great interest from a fundamental point of view. The study illuminates not only magnetic but also electronic properties of an intermediate system from a microscopic to a macroscopic one. A single atom of transition metal has a magnetic moment in a gas phase, on the other hand, a number of bulk transition metals have no magnetic moment, except Cr, Mn, Fe, Co, and Ni. This suggests that, with an increase of the size of a system consisting of magnetic atoms, magnetic moments become reduced and they are lost at an appropriate size. Such an example is found in chromium. A single crystal sample of Cr is in a sinusoidal spin density wave (SSDW) state with a maximum amplitude of $0.6\mu_B$ in the ground state and the SSDW state persists up to the Neél temperature, T_N ($=312$ K).[1] Polycrystalline samples,[2,3] fine particles,[4–6] surfaces of Cr,[7] and Cr-based alloys,[8] however, are magnetic above T_N and have enhanced magnetic moments, compared with those of single crystals. The origin is in bond-breaking due to a reduction of the coordination number of a Cr atom.[9,10] For example, in CrAl alloys,[8] Al atoms are supposed to be vacancies, as concerned with magnetic state, so Al atoms bring the bond-breaking effect to the neighboring Cr atoms. Several first-principle electronic structure calculations[11–15] have been carried out on the ground states of transition metal thin films with use of the local spin density approximation (LSDA).[16] Magnetic moments are found to be enhanced on surfaces, compared with them on the center layer which is supposed to be in a bulk state.

A single atom with an odd number of electrons has a magnetic moment in a gas phase, too. A typical example is an alkali metal atom, which has an atomic structure with a closed shell plus an s electron. However, both alkali metal crystals and surfaces are not magnetic. This suggests a possibility that, in a system consisting of alkali metal atoms, magnetic moments appear or disappear and the magnetic structure can change as a function of the size and the shape of the system. Such a possibility can be studied in a systematic way, by calculating the electronic structures of thin films with a metallic electron density as a function of the film thickness. Lang and Kohn[17–19] calculated work functions and surface energies in semi-infinite systems using the planar uniform jellium model (PUJM) on a basis of the density functional theory[20,21] with the local density approximation (LDA) applied to the exchange-correlation energy. The results show good agreement with the experimental values for alkali metals, so the theoretical treatment is expected to be suitable for investigating surface electronic structures of alkali metals. Schulte[22] applied the same approach to metallic thin films and found that the work function, i.e., the Fermi energy strongly depends on the film thickness and reveals an oscillation around the bulk Fermi energy as a function of the film thickness.

Recent observation on Au nanoparticles is very interesting: Au nanoparticles with an average diameter of about 2.5 nm are magnetic and the saturation magnetic moment attains a magnitude of $20\mu_B$ per particle.[23,24] A single Au atom has also an atomic structure with a closed shell plus an s electron, so this phenomenon is expected to be explained from the abovementioned point of view.

In the present paper, we investigate the electronic and magnetic properties of metallic thin films on a basis of the spin density functional theory within a framework of the LSDA,[16] treating the positive charge background as a planar uniform jellium. A preliminary result was previously reported by the present authors.[25] In an interacting electron gas with a uniform jellium, whether a bulk system is magnetic or not depends on r_s, which is defined by the radius of a sphere occupied by an electron. Magnetic and nonmagnetic states are favorable for larger and smaller r_s, respectively. In inhomogeneous systems, such as thin films, r_s is a function of position $\mathbf{r}$, $r_s(\mathbf{r})$. The exchange-correlation energy in the LDA and LSDA is described in terms of $r_s(\mathbf{r})$. As was shown by Lang and Kohn, there are surface dipole layers

near the surface due to a transudation of electrons from the surface.[18] $r_s(\mathbf{r})$ in the surface region is much larger than the bulk value. This leads us to a possibility of an appearance of surface magnetism in the neighborhood of the surfaces. Deep inside the thin film, the value of $r_s(\mathbf{r})$ is nearly equal to the bulk one. In such a region, magnetic state is suppressed. A compromise of such two tendencies determines whether the state over all the system is magnetic or nonmagnetic.

The theoretical treatment is discussed in Sec. II. The LSDA is applied to thin films described by the PUJM as a positive charge background. For the exchange-correlation energy for an electron, we adopt Janak-Moruzzi-Williams[26] type energy. Several states including nonmagnetic states are found as solutions of the Kohn-Sham equation.[21] The electronic and magnetic properties of such states are discussed as functions of the film thickness in Sec. III. The lowest energy state among the states is determined by comparing the total energies with one another in Sec. IV. Section V is devoted to conclusions and discussions. Hereafter we use the atomic unit in the following; with e (the magnitude of the charge on an electron), m (the mass of an electron), and $\hbar$ all set equal to unity.

II. LOCAL SPIN DENSITY APPROXIMATION IN THIN FILMS

The electronic and magnetic properties in the ground state of an interacting electron gas under an external field caused by positive charges can be represented by the spin density functional theory.[26] The electron density with spin σ at a position $\mathbf{r}$, $n_\sigma(\mathbf{r})$, in a system consisting of interacting electrons can be determined by the following equation:

$$-\frac{1}{2}\nabla^2\Psi_i^\sigma(\mathbf{r})+v_{\rm eff}^\sigma(\mathbf{r})\Psi_i^\sigma(\mathbf{r})=E_i^\sigma\Psi_i^\sigma(\mathbf{r}) \tag{1}$$

and setting

$$n_\sigma(\mathbf{r})=\sum_i |\Psi_i^\sigma(\mathbf{r})|^2, \tag{2}$$

where the sum is to be extended over the states with lower energies than the Fermi energy ϵ_F, and σ takes + or − according to the spin direction. The effective potential, $v_{\rm eff}^\sigma(\mathbf{r})$, in Eq. (1) consists of two parts; one is the electrostatic potential, $v_{\rm es}(\mathbf{r})$, not depending on σ, and the other one is the exchange-correlation potential, $v_{\rm xc}^\sigma(\mathbf{r})$, which depends on σ. $\Psi_i^\sigma(\mathbf{r})$ is the wave function of an electron with spin σ and energy eigenvalue E_i^σ.

In order to investigate metallic thin films, we adopt the PUJM as the positive charge background and take the x axis to be perpendicular to the surfaces of a film. The positive charge density $n_B(x)$ is assumed as follows:

$$n_B(x)=\begin{cases} n_0 & |x|\leqslant \frac{1}{2}D, \\ 0 & |x|>\frac{1}{2}D, \end{cases} \tag{3}$$

where D is the film thickness (see Fig. 1). The film surfaces are denoted by the planes $x=\pm D/2$. The Wigner sphere radius r_s is given by $(4\pi n_0/3)^{-1/3}$. The electronic states along the parallel directions to the surfaces, y and z, are treated as

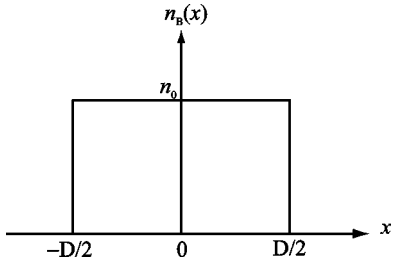

FIG. 1. Positive charge density per unit volume $n_B(x)$ in the planar uniform jellium model. n_0 is defined by $n_0=(4\pi r_s^3/3)^{-1}$. D is the film thickness. Two positions, $x=\pm D/2$, mean the surfaces.

a free electron gas. Therefore the eigenfunction $\Psi_i^\sigma(\mathbf{r})$ of Eq. (1) can be written in the following way:

$$\Psi_i^\sigma(\mathbf{r})=\Psi_{n,k_y,k_z}^\sigma(\mathbf{r})=\phi_n^\sigma(x)\exp[-i(k_y y+k_z z)] \tag{4}$$

with $n=1,2,3,\ldots$. k_y and k_z are the wave numbers along the y and z axes, respectively. Equation (1) can be rewritten in terms of $\phi_n^\sigma(x)$:

$$-\frac{1}{2}\frac{d^2}{dx^2}\phi_n^\sigma(x)+v_{\rm eff}^\sigma(x)\phi_n^\sigma(x)=\epsilon_n^\sigma\phi_n^\sigma(x), \tag{5}$$

where the eigenvalue ϵ_n^σ is called the energy level and is connected with the eigenvalue E_i^σ of Eq. (1) by relation

$$E_i^\sigma=\epsilon_n^\sigma+\frac{1}{2}(k_y^2+k_z^2). \tag{6}$$

ϵ_n^σ is the bottom of E_i^σ. ϵ_1^σ is the lowest energy among ϵ_n^σ's. Hereafter the set of states associated with ϵ_n^σ is called the ϵ_n^σ band.

The density of states for an electron with spin σ, $\rho^\sigma(\epsilon)$, is given by

$$\rho^\sigma(\epsilon)=\sum_n \rho_n^\sigma(\epsilon), \tag{7}$$

where $\rho_n^\sigma(\epsilon)$ is the partial density of states with ϵ_n^σ:

$$\rho_n^\sigma(\epsilon)=\frac{1}{2\pi}\int |\phi_n^\sigma(x)|^2 dx. \tag{8}$$

Due to the two dimensionality, $\rho_n^\sigma(\epsilon)$ is constant, $1/(2\pi)$, as a function of energy ϵ, and so $\rho^\sigma(\epsilon)$ is steplike. In Fig. 2, we show schematically the densities of states divided by the film thickness D. $\rho_n^\sigma(\epsilon)/D$ and $\rho^\sigma(\epsilon)/D$ are the partial and the total densities of states per unit volume for an electron with spin σ. $\rho_n^\sigma(\epsilon)$ is zero at $\epsilon<\epsilon_n^\sigma$ and $\rho^\sigma(\epsilon)$ is zero at $\epsilon<\epsilon_1^\sigma$. Taking into no account the surface effect, $\rho^\sigma(\epsilon_n^\sigma)/D$ is equal to $\rho_{\rm 3D}^\sigma(\epsilon_n^\sigma)$, which is the density of states of per unit volume for an electron with spin σ in a three-dimensional free electron gas at $\epsilon=\epsilon_n^\sigma$. $\rho_{\rm 3D}^\sigma(\epsilon)$ is shown by a dotted curve. An increase of D makes a decrease of $\rho_n^\sigma(\epsilon)/D$ and $\rho^\sigma(\epsilon)/D$. In the limit of $D\to\infty$, the steplike behavior in $\rho^\sigma(\epsilon)$ disappears and $\rho^\sigma(\epsilon)/D$ coincides with $\rho_{\rm 3D}^\sigma(\epsilon)$.

The electron density with spin σ, $n_\sigma(x)$, has the form

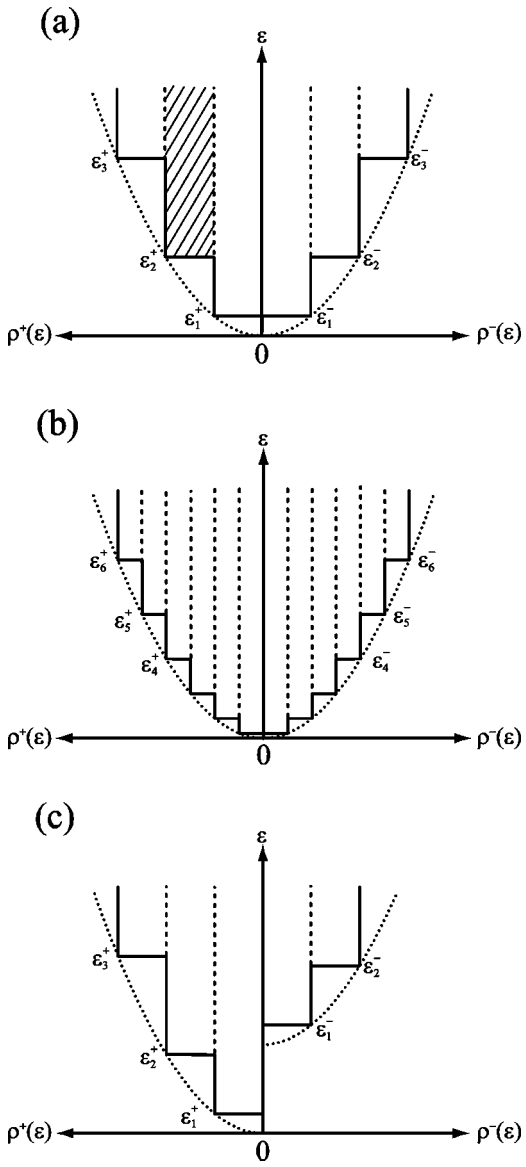

FIG. 2. Sketch of partial density of states with ϵ_n^σ per unit volume $\rho_n^\sigma(\epsilon)/D$ and total density of states per unit volume $\rho^\sigma(\epsilon)/D$. The effects of surfaces are neglected. ϵ_n^σ is the bottom of ϵ_n^σ band. $\rho_n^\sigma(\epsilon)$ is constant, $1/(2\pi)$, as a function of ϵ, due to the two dimensionality. At $D\to\infty$, $\rho^\sigma(\epsilon)/D$ coincides with the density of states per unit volume for an electron with spin σ in the three-dimensional free electron gas $\rho_{3D}^\sigma(\epsilon)$, given by a dotted curve. Three cases are shown: (a) nonmagnetic case with $D=D_0$, (b) nonmagnetic case with $2D_0$, and (c) ferromagnetic case with D_0. A hatched region in case (a) indicates the ϵ_2^+ band.

$$n_\sigma(x)=\frac{1}{2\pi}\sum_{\epsilon_n^\sigma\le\epsilon_F}(\epsilon_F-\epsilon_n^\sigma)|\phi_n^\sigma(x)|^2. \tag{9}$$

The electron density $n(x)$ and the spin density $m(x)$ are given by

$$n(x)=n_+(x)+n_-(x) \tag{10}$$

and

$$m(x)=n_+(x)-n_-(x), \tag{11}$$

respectively. The Fermi energy ϵ_F is so determined that the film keeps to be electrically neutral.

The electrostatic potential $v_{es}(x)$ depends only on x and is given by

$$v_{es}(x)=-4\pi\int_{-\infty}^{x}(x-s)[n(s)-n_B(s)]ds. \tag{12}$$

The vacuum level is chosen as zero of energy. The LSDA is applied to the exchange-correlation part of the effective potential.[16] Under this approximation, the exchange-correlation potential $v_{xc}^\sigma(x)$ is given by

$$v_{xc}^{\pm}(x)=\epsilon_{xc}+n(x)\frac{\partial\epsilon_{xc}}{\partial n(x)}\pm\frac{\partial\epsilon_{xc}}{\partial\eta(x)}[1\mp\eta(x)], \tag{13}$$

where $\eta(x)$ is the local spin polarization given by

$$\eta(x)=\frac{n_+(x)-n_-(x)}{n_+(x)+n_-(x)}=\frac{m(x)}{n(x)}. \tag{14}$$

ϵ_{xc} is the exchange-correlation energy per electron in a homogeneous electron gas. In our numerical calculation, we adopt Janak-Moruzzi-Williams type for ϵ_{xc}.[26]

The electron density, the spin density, and the effective potential are obtained by solving self-consistently Eqs. (5), (9), (12), and (13). Several magnetic states including nonmagnetic state are found, so we should compare the total energies with one another in order to determine the ground state. The total energy per surface area E_{tot} is given by

$$E_{tot}=\sum_\sigma\left\{\frac{1}{4\pi}\sum_{\epsilon_n^\sigma\le\epsilon_F}[\epsilon_F^2-(\epsilon_n^\sigma)^2]-\int v_{eff}^\sigma(x)n_\sigma(x)dx\right\}+\frac{1}{2}\int v_{es}(x)[n(x)-n_B(x)]dx+\int\epsilon_{xc}(x)n(x)dx, \tag{15}$$

where the first term is the kinetic energy E_{kin}, the second term the electrostatic energy E_{es}, and the third term the exchange-correlation energy E_{xc}.

III. ELECTRONIC AND MAGNETIC STRUCTURES

The abovementioned set of self-consistent equations (5), (9), (12), and (13), has several types of solution for a metallic thin film, as will be shown later. In the present section, the electronic and magnetic properties of each type are discussed for $r_s=6$, as an example.

A. Nonmagnetic state

Following Schulte's work,[22] we first discuss nonmagnetic (N) state, in which the spin density $m(x)$ is identical to zero. Nonmagnetic solutions can be found for all D's. The energy level ϵ_n $(=\epsilon_n^+=\epsilon_n^-)$ and the Fermi energy ϵ_F as functions of D are plotted in Fig. 3(a). We can see three important findings from this figure. One is that, in the limit of $D\to0$, ϵ_F and all ϵ_n's approach zero which is the energy of the vacuum level, due to no positive charge background at $D=0$. Another one is that ϵ_F approaches the bulk value in the limit of $D\to\infty$. The other one is the most striking; all ϵ_n's and ϵ_F as

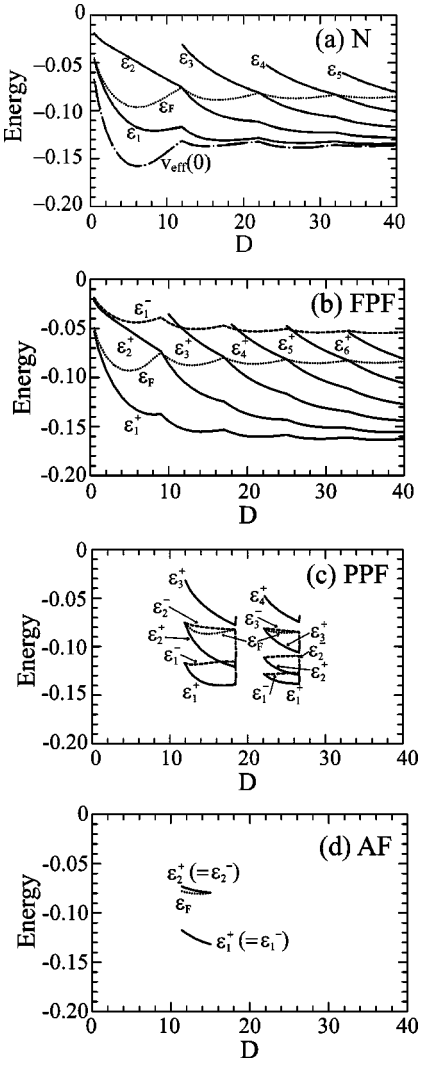

FIG. 3. Energy levels ϵ_n^σ's and Fermi energy ϵ_F as functions of D for $r_s=6$. Four states are shown; (a) nonmagnetic (N) state, in which $\epsilon_n=\epsilon_n^+=\epsilon_n^-$. A dot-dashed curve means the effective potential at the origin $v_{\rm eff}(0)$ $[=v_{\rm eff}^+(0)=v_{\rm eff}^-(0)]$, (b) fully polarized ferromagnetic (FPF) state, in which only ϵ_n^+ bands are occupied and ϵ_n^- bands remain unoccupied, (c) partially polarized ferromagnetic (PPF) state, in which a lager number of bands with + spin are occupied, and (d) antiferromagnetic (AF) states, in which $\epsilon_n^+=\epsilon_n^-$.

functions of D have cusps at the intersecting points of the ϵ_F curve with the ϵ_n curves. Now we consider the origin of this phenomenon. At $D=0$, all ϵ_n's and ϵ_F are supposed to be zero. With an increase of D, the number of electrons in the film increases proportionally to D, accompanied with lowering of all ϵ_n's and ϵ_F. The difference $\epsilon_F-\epsilon_1$, has to increase proportionally to D, because the total density of states, $\rho(\epsilon)$ $[=2\rho^+(\epsilon)=2\rho_1^+(\epsilon)]$, is constant as a function of ϵ due to the two dimensionality. As the effective potential width extends with D, the lowering of ϵ_1 becomes slowly, so ϵ_F is increased in order to accommodate an increment of electrons due to an increase of D. ϵ_1, however, cannot continue to be lowered, as can be understood from a fact that the energy levels in a square well potential are lowered with an increase of the well width but the lowest energy level cannot be lower than the bottom of the well. After then, ϵ_1 turns to be increase, because the electrostatic potential is elevated due to a

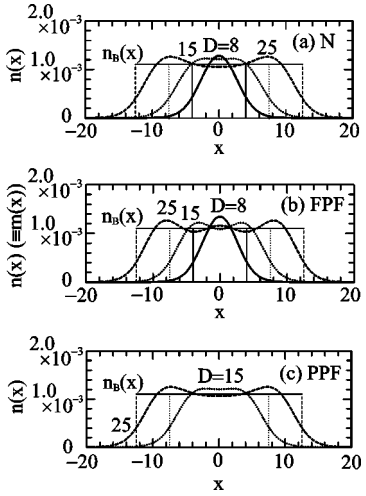

FIG. 4. Electron density profiles in (a) N, (b) FPF, and (c) PPF. In FPF, the electron density is identical to the spin density $[n(x)=m(x)]$.

decrease of transudation of electrons from surfaces, in other word, the effective potential is increased, as is see from Fig. 3(a), where $v_{\rm eff}(0)$ $[=v_{\rm eff}^+(0)=v_{\rm eff}^-(0)]$ is plotted. This leads us to a rapid increase of ϵ_F and to an occupation of the ϵ_2 band in addition to the ϵ_1 band at $D=11.9$. As soon as ϵ_2 becomes under ϵ_F, the density of states is doubled, compared with that at $\epsilon_2>\epsilon_F$, so ϵ_1, ϵ_2, and ϵ_F turn to be lowered again. Therefore we can find a cusp in ϵ_n's and ϵ_F as functions of D. Such a situation can be also found at $D=22.1,32.0,\ldots$. The cusp, however, becomes difficult to be observed with an increase of D, and then disappears in the limit of $D\to\infty$. The reason is; when ϵ_{n+1}-band begins to be occupied at the nth cusp, the relative portion of the contribution to the total density of states is $1/(n+1)$ and it approaches zero in the limit of $D\to\infty$.

The wave function $\phi_n(x)$ $[=\phi_n^+(x)=\phi_n^-(x)]$ has $(n-1)$ nodes, and the partial electron density profile with ϵ_n has an n-peak structure. The electron density profiles and the corresponding effective potentials for $r_s=6$ are shown in Figs. 4(a) and 5(a), where $D=8$, 15, and 25. For $D=8$, $n(x)$ has a single-peak structure due to only ϵ_1 band occupation and $v_{\rm eff}(x)$ $[=v_{\rm eff}^+(x)=v_{\rm eff}^-(x)]$ has a single minimum. For $D=15$, a clear double-peak structure cannot be found in $n(x)$, although $v_{\rm eff}(x)$ has a double-minimum structure, because of small $\epsilon_F-\epsilon_2$, i.e., only a little occupation of the ϵ_2 band. For $D=25$, $n(x)$ has a double-peak structure, although $v_{\rm eff}(x)$ has a clear triple-minimum one. With an increase of the number of occupied bands with D, the electron density at a position distant from the surfaces approaches a constant value n_0. In the limit of $D\to\infty$, the electron density coincides with the positive charge density n_0 except the neighborhoods of the surfaces, where the Friedel oscillation is found. The Friedel oscillation produces the surface dipole layers.[18]

B. Fully polarized ferromagnetic state

As ferromagnetic solutions, we find two states; one is fully polarized ferromagnetic (FPF) state, where only bands with + spin can be occupied and all bands with − spin

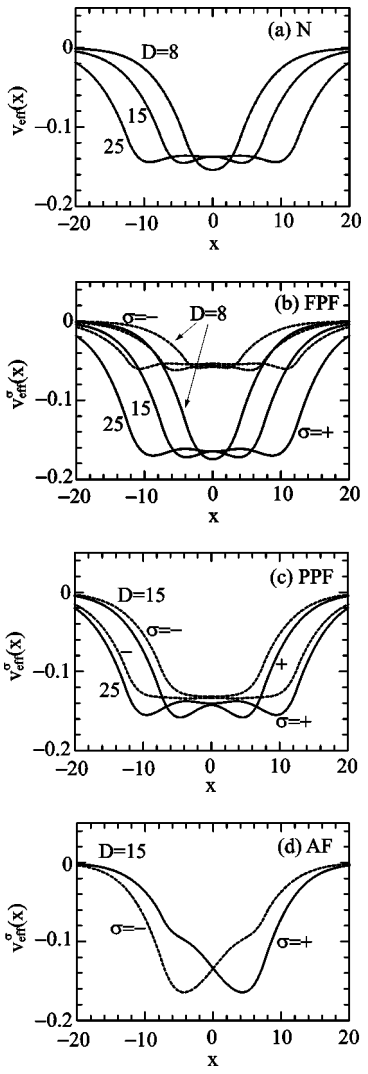

FIG. 5. Effective potentials in (a) N, in which $v_{\rm eff}(x)=v^{+}_{\rm eff}(x)=v^{-}_{\rm eff}(x)$, (b) FPF, (c) PPF, and (d) AF. In all cases, solid and dashed curves mean $v^{+}_{\rm eff}(x)$ and $v^{-}_{\rm eff}(x)$, respectively. In AF, the energy levels, ϵ^{+}_{n} and ϵ^{-}_{n}, are degenerate, and the wave function for an electron with $+$ $(-)$ spin has a larger amplitude in the positive (negative) region. $v^{+}_{\rm eff}(x)$ and $v^{-}_{\rm eff}(x)$ in AF are symmetric with respect to $x=0$.

remain unoccupied. The other one is partially polarized ferromagnetic (PPF) state, where bands with $+$ spin and with $-$ spin are unequally occupied. In the present subsection, FPF state is discussed.

The energy levels, ϵ^{+}_{n} and ϵ^{-}_{n}, and the Fermi energy ϵ_F as functions of D are shown in Fig. 3(b). The range of existence of the FPF state is extended over all D's. In the limit of $D\rightarrow 0$, both ϵ^{+}_{1} and ϵ_F are supposed to approach zero. The difference $\epsilon_F-\epsilon^{+}_{1}$ is increased proportionally to D. The proportional coefficient is two times that in the N state, because the density of states in the FPF state is a half of that in the N state. The bottom of the effective potential in the FPF state is lower than in the N state, due to more lowering of the exchange-correlation potential, compared with that in the N state, as is seen from Figs. 5(a) and 5(b). ϵ_F turns to increase at a smaller D than in the N state, and the first cusp appears at a smaller D than that in the N state, too. In the present case, the position of the first cusp is found at $D=9.0$, where

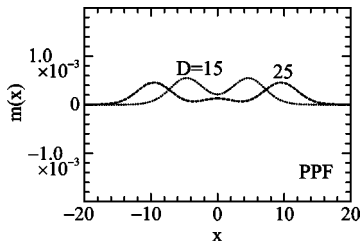

FIG. 6. Spin density profiles in PPF at $D=15$ and 25.

the ϵ^{+}_{2} band becomes occupied in addition to the ϵ^{+}_{1} band, but the other ϵ^{+}_{n} bands and all bands with $-$ spin remain unoccupied. In the same way, ϵ^{+}_{3}, ϵ^{+}_{4}, ϵ^{+}_{5}, ϵ^{+}_{6}, ..., becomes lower than ϵ_F, and cusps appear successively.

Several example of the electron density profiles, which are identical to the spin density profiles $[m(x)=n(x)]$ in the FPF state, are shown in Fig. 4(b), and the corresponding effective potentials, $v^{\sigma}_{\rm eff}(x)$, are shown in Fig. 5(b). $n(x)$ has a single-, a double-, and a triple-peak structures for $D=8$, 15, and 25, respectively. The structures are very clear compared with cases in the N state, reflecting the corresponding effective potentials for an electron with $+$ spin, $v^{+}_{\rm eff}(x)$'s, which have a single-, a double-, and a triple-minimum structures, respectively.

C. Partially polarized ferromagnetic state

PPF solutions are found at $11.9\leqslant D\leqslant 18.4$ and $22.2\leqslant D\leqslant 27.6$, as is shown in Fig. 3(c). In the former region, the ϵ^{+}_{1}, ϵ^{+}_{2}, and ϵ^{-}_{1} bands are occupied and the other bands are unoccupied, on the other hand, in the latter case, only the ϵ^{+}_{1}, ϵ^{+}_{2}, ϵ^{+}_{3}, ϵ^{-}_{1}, and ϵ^{-}_{2} bands are occupied. Another type of PPF state can be expected, however, we could not find it for $r_s=6$. With an increase of D, the PPF state appears at the intersecting point of the ϵ_2 curve with the ϵ_F curve in the N state, in other words, the degenerate ϵ_1 and ϵ_2 bands split off into ϵ^{+}_{1} and ϵ^{-}_{1} bands and into ϵ^{+}_{2} and ϵ^{-}_{2} bands, respectively, and then the PPF state disappears suddenly at the intersecting point of the ϵ^{-}_{2} curve with the ϵ_F curve in the PPF state. The same situation is found in the latter case.

Examples of $n(x)$ and $m(x)$ are shown in Figs. 4(c) and 6, respectively. The electron density profiles are very similar to the corresponding profiles in the N state, because of small exchange splitting. The spin density is found to be localized near the surfaces, as is seen from those of $D=15$ and 25. The difference, $v^{-}_{\rm eff}(x)-v^{+}_{\rm eff}(x)$, is small compared with the FPF case, as is seen from Fig. 5(c).

D. Antiferromagnetic state

Antiferromagnetic (AF) states are found in $11.5\leqslant D\leqslant 15.0$, as is shown in Fig. 3(d). Two bands, ϵ^{+}_{1} and ϵ^{-}_{1} bands, are occupied and the other bands are unoccupied. Of course, ϵ^{+}_{1} and ϵ^{-}_{1} are equal to each other, so they are equivalently occupied. The wave functions $\phi^{+}_{1}(x)$ and $\phi^{-}_{1}(x)$ have large amplitudes in a positive and negative regions of x, respectively, as is seen from $v^{+}_{\rm eff}(x)$ and $v^{-}_{\rm eff}(x)$ plotted in Fig. 5(d). $n(x)$ and $m(x)$ are shown in Figs. 7 and 8, respectively. The electron density profiles in the AF and the FPF states are very similar to each other, and the spin

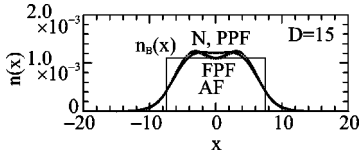

FIG. 7. Electron density profiles at $D=15$. The profiles in N and PPF have very similar forms to each other, and the densities in FPF and AF have very similar profiles to each other.

density profiles are also seemed to be similar to each other except the neighborhood of $x=0$, if the sign of the spin density at a negative value of x in the AF state is reversed. This gives us one physical description concerned with a formation of FPF and AF states at $D=15$; an FPF film with $D=15$ consists of two FPF films with $D=7.5$, which have parallel spin densities to each other, on the other hand, an AF film consists of two FPF films with $D=7.5$, in which the spin directions in two FPF films are antiparallel. The minimum value of D, at which we can obtain AF state, is 11.5 for $r_s=6$. At a smaller D than this value, only FPF and N states are obtained. This suggests that there exists a minimum size of the film width for forming AF state.

IV. GROUND STATE

In order to determine the ground state of a thin film, we compare the total energies in N, FPF, PPF, and AF states with one another. The total energies per unit volume, $E_{\rm tot}/D$, as a function of D are shown in Fig. 9, where $r_s=6$. The lowest energy state changes as a function of D; FPF at $D \leqslant 9.0$, N at $9.0<D\leqslant 11.9$, PPF at $11.9<D\leqslant 12.8$, FPF at $12.8<D\leqslant 16.4$, PPF at $16.4<D\leqslant 17.1$, N at $17.1<D \leqslant 22.1$, PPF at $22.1<D\leqslant 25.6$, and N at $25.6<D$. The AF state has always higher energy than the other states for a given D. As is seen from Fig. 10, magnetic states have higher kinetic energies and lower exchange-correlation energies than nonmagnetic states. The electrostatic energy is smaller than the other energies by about tenth order.

The most striking phenomenon is the ground state is FPF in sufficiently thin films, for example, when D is smaller than 9.0 at $r_s=6$. When D is increased from 0, the energy in the FPF state becomes higher than that in the N state at $D>D_C$ shown by an arrow in Fig. 9. D_C is decreased with a decease of r_s. Figure 11 shows the phase diagram of the ground state. The phase boundary between FPF and N states, given by a solid curve, means D_C as a function of r_s. When r_s is decreased, we suppose that D_C approaches zero. If D/r_s is small, the ground state is FPF, whatever value r_s takes.

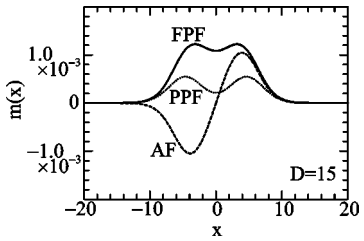

FIG. 8. Spin density profiles in FPF, PPF, and AF at $D=15$. The spin density profiles in FPF and AF films with $D=15$ is expected to consist of two FPF films with $D=7.5$.

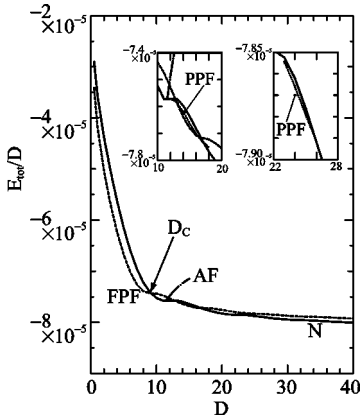

FIG. 9. Total energy per unit volume as a function of D. The ground state is FPF at a smaller D than D_C indicated by an arrow.

So far we have discussed the electronic and magnetic properties of metallic thin films under an assumption that the number of electrons in a thin film is proportional to D. Here we consider another case; the electron number per unit area n_0D is constant as a function of D. In other words, the positive charge density is proportional to the inverse of D. The total energy per unit area $E_{\rm tot}$ in the FPF state is always the lowest for $D<D_C$, as is shown in Fig. 12, where n_0D is fixed to 0.009. Both in the limit of $D\rightarrow 0$ and in the limit of $n_0\rightarrow 0$, $E_{\rm tot}$ approach to be zero. Therefore, there should exist the minimum value $E_{\rm tot}$. This means that there is an appropriate electron density, at which the total energy is lowest as a function of n_0. The electron density with the lowest energy is 0.001125 at $D=8$.

V. CONCLUSIONS AND DISCUSSIONS

We have investigated the electronic and magnetic properties of metallic thin films using the LSDA applied to the PUJM. Several important results are obtained as follows. (1) There are nonmagnetic (N), fully polarized ferromagnetic (FPF), partially polarized ferromagnetic (PPF), and antiferromagnetic (AF) states. (2) Magnetic moments in the PPF state appear in the neighborhoods of the surfaces in thin films with metallic electron density. (3) An AF film with the film thickness D consists of two FPF films with $D/2$. (4) The

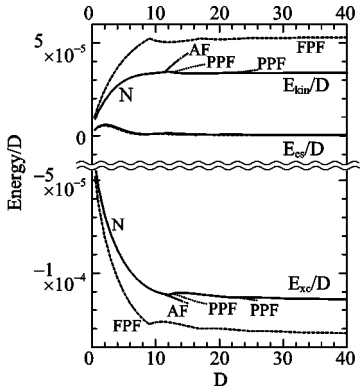

FIG. 10. Contributions of kinetic, electrostatic, and exchange-correlation parts to total energy per unit volume as functions of D. The electrostatic part is very small in all cases. FPF state is the most favorable due to large gain of exchange-correlation energy.

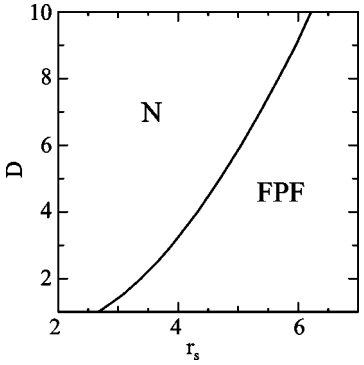

FIG. 11. Phase diagram for very thin films with $D \leqslant 10$. The phase boundary between FPF and N is indicated by D_C.

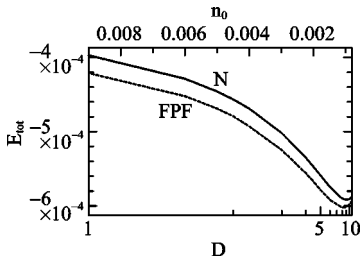

FIG. 12. Total energy per unit area in FPF and N as a function of D, calculated under the condition that the electron number contained in unit area is fixed ($n_0 D = 0.009$). The ground state is FPF. Both FPF and N states have the lowest energy at $D = 8.0$ and 9.0, respectively.

ground state is varied as a function of D. (5) The AF state is not favorable. (6) If D/r_s is small, the ground state is FPF, whatever value r_s takes.

We have found N and FPF states for all D's, and PPF and AF states for an appropriate range of D as solutions of the Kohn-Sham equation. Magnetic ground states appear in thin films. The origin is in the fact that, in a three-dimensional free electron gas, the ground state is magnetic for low electron density, and nonmagnetic for high electron density.[27] As was shown in Figs. 4 and 7, however, the electron density of a thin film deviates largely from the positive charge background in the neighborhoods of surfaces, due to the transudation of electrons form the surfaces. In such regions, the electron density becomes smaller than the average value n_0, so the surface region have a tendency to have a finite spin polarization. Going deep inside the film, the electron density reveals a damped oscillation around the positive charge density n_0. The finite spin density is reduced and disappears in a region distant from the surfaces. Such two tendencies compromise in the film, and whether the system is nonmagnetic or magnetic is determined as a function of D. For films with large D, a nonmagnetic region appearing deep inside the film prevails over magnetic regions near the surfaces, so the nonmagnetic state is expected over the film, on the other hand, for films with small D, the surface-induced magnetic state is capable to survive inside the film.

The AF states are found in $11.5 \leqslant D \leqslant 15.0$. This reflects the following fact: there exists a minimum size in film width D for an appearance of some structure except a single-peak one in the electron density profile. As was abovementioned, the electron density profiles in FPF and AF states are very similar and the spin density profiles are similar except around $x = 0$, if the sign of the spin density in the negative region of x is reversed. In the FPF state, ϵ_1^+ and ϵ_2^+ bands are occupied, on the other hand, in the AF state, ϵ_1^+ and ϵ_1^- bands are occupied. In both cases, two bands are occupied. This leads us to a formation of double-peak structure in the electron density profile. If only one band is occupied, such a structure can never be observed, so the necessary condition for an appearance of some structure except single-peak one is that, at least, two bands are occupied. The number of occupied bands are increased with an increase of the number of electrons in the film, i.e., with an increase of D. Therefore there exists a minimum size of D as a condition for having an electron density profile with more than one peak structure. In FPF state, the spin density profile is identical to the electron density profile, so the abovementioned condition must be satisfied for finding a multipeak structure in the spin density profile. The AF state is nearly fully polarized except around $x = 0$, so the abovementioned condition must be satisfied for finding an AF state, too. Therefore a film with D larger than the minimum size can be AF.

If a film is very thin, it is in a FPF state. It is expected that this conclusion does not depend on exchange-correlation energy applied, such as von Barth-Hedin,[16] Janak-Moruzzi-Willimas,[26] Gunnarsson-Lundqvist,[28] and Perdew-Zunger[29] types. In addition, it is expected that the conclusion does not depend on approximation applied, for example, the LSDA or the generalized gradient approximation (GGA).[30] The reason is: in very thin films, the local r_s is effectively very large due to a large transudation of electrons from the film, so magnetic state is energetically the most favorable.

The electronic structure calculations for transition metal thin films and surfaces, such as Cr, Fe, and Ni, have been carried out by using the full-potential linearized augmented plane wave method[11–15] based on the first principle. In these calculations, a remarkable d-band narrowing effect has been found on the surface, due to a reduction of coordination number of a surface atom. This leads us to an appearance or an enhancement of magnetic moments on surface atoms, compared with those in bulk crystals. The surface magnetism is realized by the bond-breaking effect. On the other hand, in the present system, the transudation of electrons from surfaces brings us an appearance of surface magnetic moments.

It is well known that the electronic structure of alkali metals can be well described by a free electron gas with a uniform jellium model. This fact is confirmed by the electronic structure calculation based on the first principle.[31] Moreover, it is shown that the surface electronic structures can be described by the free electron gas model with the PUJM.[17–19] Therefore, our conclusion is at least semiquantitatively correct, so alkali metal thin films, especially Rb and Cs thin films are expected to be magnetic. A very recent observation[32] on giant magnetic moments of Fe and Co on and in Cs films supports our prediction. The giant magnetic moments attain about $8\mu_B$ per Co atom and $7\mu_B$ per Fe atom, similar to the giant moment of Fe in Pd.[33] The origin of this phenomenon is in a nearly ferromagnetic state found in very thin films of Cs in our calculation. The thickness-dependence of the giant moments should be investigated in detail. It is expected that the films of Cs with Co and Fe

impurities become to have larger magnetic moments with decreasing the film thickness.

Recently nanoparticles of Au with an average diameter of about 2.5 nm have been reported to be magnetic.[23,24] The saturation magnetic moment per particle is about $20\mu_B$. An appearance of magnetism in Au metals and Au surfaces has not reported. However, a single Au atom has an atomic structure of a closed shell plus an *s* electron. This phenomenon can be explained within our conclusion. In a nanoparticle of Au with a diameter of 2.5 nm, the portion of surface atoms to all atoms in sphere is about 1/2. Therefore the nanoparticle has a tendency to become more magnetic than thin films. The magnetic moments are expected to be localized near the surface of the particle.

Several theoretical studies have appeared on the magnetic properties of double quantum wells.[34,35] Each of wells forming the double wells is supposed to correspond to a metallic thin film mentioned above, although the positive charges are differently arranged from the present case. For example, in AlGaAs/GaAs,[34] r_s is about 3.5 in unit of the effective Bohr radius. A single well with width smaller than 2.2 is expected to be FPF, as is seen from Fig. 11. It is expected that the ground state is varied as a function of the width, as was mentioned in Sec. IV.

[1] S.A. Werner, A. Arrott, and H. Kendrich, Phys. Rev. **155**, 528 (1967).
[2] G.E. Bacon and H. Cowlam, J. Phys. C **2**, 238 (1969).
[3] P.E. Ferguson, J. Appl. Phys. **49**, 2203 (1978).
[4] S. Matsumoto and I. Nishida, J. Phys. Soc. Jpn. **49**, 1005 (1980).
[5] K. Nakahigashi, K Watari, M. Kogachi, and S. Minamigawa, J. Phys. Soc. Jpn. **61**, 154 (1992).
[6] Y. Teraoka and Y. Tabata, Surf. Sci. **271**, 308 (1992).
[7] L.E. Klebanoff, S.W. Pobey, G. Liu, and D.A. Shirley, Phys. Rev. B **30**, 1048 (1984).
[8] S. Arajs, N.L. Reeves, and E.E. Anderson, J. Appl. Phys. **42**, 1691 (1971).
[9] Y. Teraoka and J. Kanamori, Inst. Phys. Conf. Ser. **39**, 588 (1978).
[10] G. Allan, Phys. Rev. B **19**, 4774 (1979).
[11] S. Ohnishi, A.J. Freeman, and M. Weinert, Phys. Rev. B **28**, 6741 (1983).
[12] E. Wimmer, A.J. Freeman, and H. Krakauer, Phys. Rev. B **30**, 3113 (1984).
[13] C.L. Fu, A.J. Freeman, and T. Oguchi, Phys. Rev. Lett. **54**, 2700 (1985).
[14] C.L. Fu and A.J. Freeman, Phys. Rev. B **33**, 1755 (1986).
[15] A.J. Freeman and R. Wu, Prog. Theor. Phys. **106**, 387 (1991).
[16] U. von Barth and L. Hedin, J. Phys. C **5**, 1629 (1972).
[17] N. D. Lang, *Solid State Physics*, edited by F. Seitz, D. Turnbull, and H. Ehrenreich (Academic, New York, 1973), Vol. 28, p. 255.
[18] N.D. Lang and W. Kohn, Phys. Rev. B **1**, 4555 (1970).
[19] N.D. Lang and W. Kohn, Phys. Rev. B **3**, 1251 (1970).
[20] P. Hohenberg and W. Kohn, Phys. Rev. **136**, B864 (1964).
[21] W. Kohn and L.J. Sham, Phys. Rev. **140**, A1133 (1965).
[22] F.K. Schulte, Surf. Sci. **55**, 427 (1976).
[23] Y. Nakae, Y. Seino, T. Teranishi, M. Miyake, S. Yamada, and H. Hori, Physica B (to be published).
[24] H. Hori, T. Teranishi, Y. Nakae, Y. Seino, M. Miyake, and S. Yamada, Phys. Lett. (to be published).
[25] K. Okazaki and Y. Teraoka, Surf. Sci. **433-435**, 672 (1999).
[26] J.F. Janak, V.L. Moruzzi, and A.R. Williams, Phys. Rev. B **12**, 1257 (1975).
[27] D.M. Ceperley and B.J. Alder, Phys. Rev. Lett. **45**, 565 (1980).
[28] O. Gunnarsson and B.I. Lundqvist, Phys. Rev. B **12**, 1257 (1975).
[29] J.P. Perdew and A. Zunger, Phys. Rev. B **23**, 5048 (1981).
[30] J.P. Perdew, J.A. Chevary, S.H. Vosko, K.A. Jackson, M.R. Pederson, D.J. Singh, and C. Fiolhais, Phys. Rev. B **46**, 6671 (1992).
[31] V. L. Moruzzi, J. F. Janak, and A. R. Williams, *Calculated Electronic Properties of Metals* (Pergamon Press, New York, 1978).
[32] H. Beckmann and G. Bergmann, Phys. Rev. Lett. **83**, 2417 (1999).
[33] G. Bergmann, Phys. Rev. B **23**, 3805 (1981).
[34] F.A. Reboredo and C.R. Proetto, Phys. Rev. Lett. **79**, 463 (1997).
[35] R.J. Radtke, P.I. Tamborenea, and S. das Sarma, Phys. Rev. B **54**, 13 832 (1996).